Blue Globe Report

Erneuerbare Energien #9/2015

Solution-based low cost photovoltaics

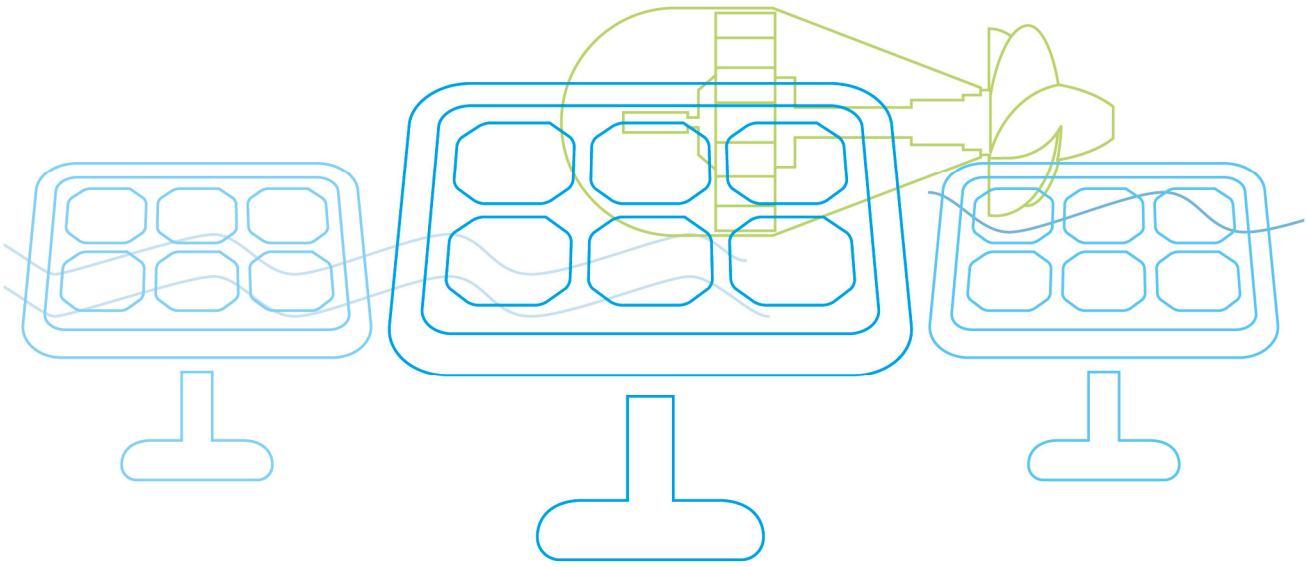

Theodoros Dimopoulos et al.

VORWORT

Die Publikationsreihe BLUE GLOBE REPORT macht die Kompetenz und Vielfalt, mit der die österreichische Industrie und Forschung für die Lösung der zentralen Zukunftsaufgaben arbeiten, sichtbar. Strategie des Klima- und Energiefonds ist, mit langfristig ausgerichteten Förderprogrammen gezielt Impulse zu setzen. Impulse, die heimischen Unternehmen und Institutionen im internationalen Wettbewerb eine ausgezeichnete Ausgangsposition verschaffen.

Jährlich stehen dem Klima- und Energiefonds bis zu 150 Mio. Euro für die Förderung von nachhaltigen Energie- und Verkehrsprojekten im Sinne des Klimaschutzes zur Verfügung. Mit diesem Geld unterstützt der Klima- und Energiefonds Ideen, Konzepte und Projekte in den Bereichen Forschung, Mobilität und Marktdurchdringung.

Mit dem BLUE GLOBE REPORT informiert der Klima- und Energiefonds über Projektergebnisse und unterstützt so die Anwendungen von Innovation in der Praxis. Neben technologischen Innovationen im Energie- und Verkehrsbereich werden gesellschaftliche Fragestellung und wissenschaftliche Grundlagen für politische Planungsprozesse präsentiert. Der BLUE GLOBE REPORT wird der interessierten Öffentlichkeit über die Homepage www.klimafonds.gv.at zugänglich gemacht und lädt zur kritischen Diskussion ein.

Der vorliegende Bericht dokumentiert die Ergebnisse eines Projekts aus dem Forschungs- und Technologieprogramm „Neue Energien 2020“. Mit diesem Programm verfolgt der Klima- und Energiefonds das Ziel, durch Innovationen und technischen Fortschritt den Übergang zu einem nachhaltigen Energiesystem voranzutreiben.

Wer die nachhaltige Zukunft mitgestalten will, ist bei uns richtig: Der Klima- und Energiefonds fördert innovative Lösungen für die Zukunft!

Ingmar Höbarth
Geschäftsführer, Klima- und Energiefonds

Theresia Vogel
Geschäftsführerin, Klima- und Energiefonds

Solution-based low cost photovoltaics

SOLO-PV

AutorInnen:
Theodoros Dimopoulos, AIT
Stephan Abermann, AIT
Rachmat Adhi Wibowo, AIT
Yaroslav Romanyuk, EMPA
Melanie Werner, EMPA
Anneliese Pönninger, EVG

1 Inhaltsverzeichnis

1 Inhaltsverzeichnis 4
2 Einleitung 5
3 Inhaltliche Darstellung 6
4 Ergebnisse und Schlussfolgerungen 22
5 Ausblick und Empfehlungen 23
6 Literaturverzeichnis 24
7 Kontaktdaten 24

2 Einleitung

The various solar PV technologies such as crystalline silicon (c-Si) and thin film solar cells (TFSC) differ significantly in their production process. c-Si is strongly dependent on the production of ingots and wafers. Cell producers apply various coatings to the wafers and subsequently contacts to the cells. These cells are then assembled by module manufacturers into strings, laminated and framed. Finally, system integrators and installers carry out design and install the completed PV systems. In the case of TFSC technologies, the costly absorber materials are usually deposited by physical or chemical methods on substrates like glass, polymer or metal foils, and the single cells are monolithically integrated and serially connected directly after the deposition processes to form the module. Hence, no ingot/wafer production and no module assembly is necessary, merging these three parts of the value chain to one.

The *International Energy Agency PV Technology Roadmap* summarized the main industry manufacturing aspects and R&D areas for the current and possible up-coming PV thin film technologies until 2030. Any new successful TFSC concept should address as much as possible of these issues in order to be able to compete with the current main players of CIGS, and CdTe. SOLO-PV was the first stage of a project chain, which aims to address the manufacturing aspects and R&D issues as identified by the IEA:

- **Industry manufacturing aspects**
  - Simplified production processes
  - Management of toxic materials
  - Improved deposition techniques
  - Large, high-efficiency production units
  - Availability of manufacturing materials
- **Selected R&D areas**
  - Improved cell structures
  - Improved deposition techniques
  - Advanced materials and concepts

The subjects of focus in SOLO-PV were: (a) The development of novel, flexible, and cost-effective solution-based fabrication processes for 3rd generation thin-film photovoltaics. (b) R&D regarding such production methods with the help of the very promising “material system” Cu_2ZnSnS/Se_4 (“CZTS/Se” or “kesterite”) incorporating solely non-toxic and abundant materials. (c) Creation of a functional “laboratory-scale” solar cell device for the conversion of solar light into electricity.

The SOLO-PV project was a 3-year collaborative project with two research partners, the AIT-Austrian Institute of Technology and the EMPA – Laboratory for Thin Films and Photovoltaics and one industrial partner, the EVG. The project work was distributed in 5 workpackages (WPs). Each WP from 1-3 had to do with the development of an individual material component needed for the construction of the kesterite absorber solar cell. WP1 had to do with the kesterite absorber itself, WP2 with the “buffer” layer (an n-type high bandgap semiconductor), WP3 with the transparent conductive oxide. In WP4 the individual material components were assembled into a solar cell and this was characterized with regard to its photovoltaic performance. WP5 concerned the project management and dissemination of the results. The project focus was clearly on the processing side of materials development, investigating low-cost, solution-based processes such as chemical spray pyrolysis (CSP), electrochemical deposition

(ECD) and chemical bath deposition. Vacuum-based deposition techniques were only used as supportive techniques for certain “standard” materials such as the Mo-coated glass substrates.

3 Inhaltliche Darstellung

Below we give the main results of our investigations on the specific subtasks of the project, categorized into individual materials and processes:

Kesterite absorber by ultrasonic spray pyrolysis (USP): This approach was pursued at EMPA. CZTS and Zn/Sn/S thin films were grown by USP in a system with two ultrasonic nebulizers operating at 1.7MHz. CZTS films were sprayed onto cleaned soda lime glass (SLG) or Mo/SLG substrates. 600 nm Mo was deposited by DC sputtering. Cupric chloride $CuCl_2$ or cupric acetate $Cu(CH3COO)_2$ were dissolved in ethanol to form the first Cu- containing solution. Monoethanolamine was added to the ethanol solution to improve the solution solubility. The second solution was prepared by dissolving Zinc chloride ZnCl2, stanic chloride $SnCl_4$, thiourea $SC(NH_2)_2$ TU or thioacetamide C_2H_5NS TAA in acetone with total molarity of 0.25-0.4 M. Lactic acid $C_3H_6O_3$ was added to the Zn/Sn/S precursor solution. The two precursor solutions were sprayed in the sequence Cu- and then Zn/Sn/S-containing solutions.

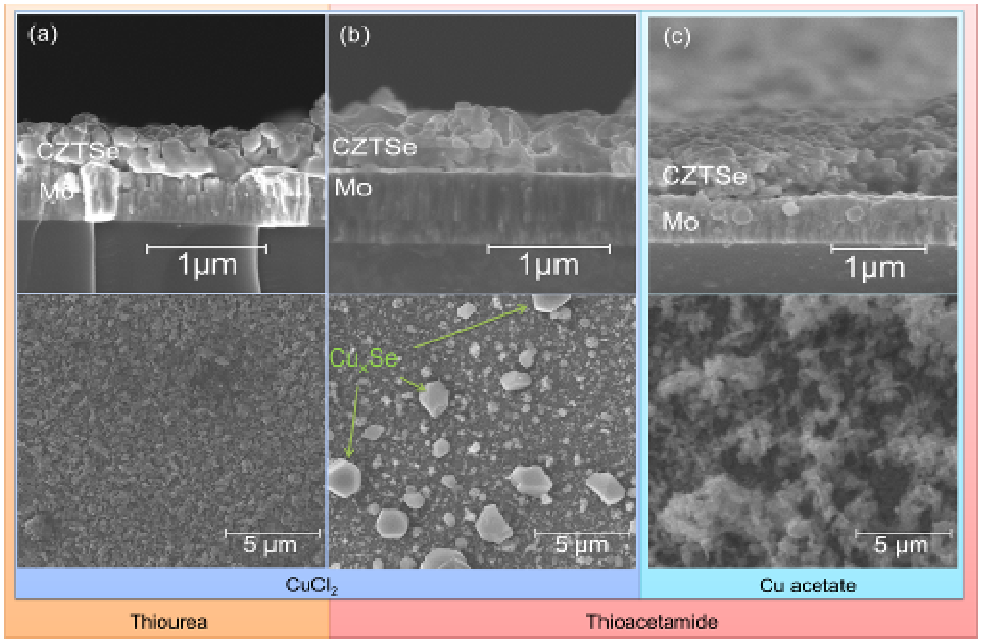

Fig 1. (a-c) SEM cross sectional images and the according top views below of CZTSe films. (a) Initial solution with CuCl2 and TU, (b) with CuCl2 and TAA and (c) with Cu(CH3COO)2 and TU as listed in table 1.

The temperature was set to 370 °C and nitrogen was used as carrier gas. The spraying rate was fixed at 1.6 ml/min resulting in an average film thickness of ~800 nm after 30 min. The Zn/S/Sn solution was deposited on both SLG and Mo/SLG substrates. In order to reduce the cooling effect during the spraying, the deposition was done by one directional scanning of the funnel. After spraying, the CZTS precursors were selenised in a two-zone tube furnace with a N_2 atmosphere for 35 min, keeping the temperature in the selenium zone at 370 °C and 600 °C at the substrate zone. The compositional ratio of the CZTSe and Zn/Sn/S layers where measured by X-ray fluorescence (XRF) and energy dispersive X-ray (EDX) spectroscopy. Morphology was studied by scanning electron microscopy (SEM) and phase analysis was done by X-ray diffraction (XRD).

The effect of different copper salts on the film morphology was studied and the cross-sectional SEM images of annealed CZTSe films with different Cu salts and TU/TAA are shown in Fig.1 (a-c). Fig.1a contained CuCl2 and TU in the precursor solution and its initial precursor composition is displayed in Table 1. In the same manner Fig.2b shows a CZTSe film prepared from CuCl2 in the first solution, and TAA and Sn, Zn salts in the second solution (sample B) and Fig.2c Cu acetate and TAA (sample C). Samples A and B are similar in their crystallinity while sample C shows a more porous, nanocrystalline structure. The film thickness for the samples using TAA is slightly increased (A:650nm, B:750nm, C:800nm). Apparently cupric acetate has a negative effect on the grain size and promotes roughness.

Sample name	Cu [M]	Zn [M]	Sn [M]	TU [M]	TAA [M]	Cu/(Zn+Sn)	Zn/Sn
A	0.2 $CuCl_2$	0.12	0.04	0.34	-	0.69	0.71
B	0.2 $CuCl_2$	0.2	0.04	-	0.24	0.69	1.67
C	0.2 $Cu(CH_3COO)_2$	0.2	0.05	-	0.25	1.04	1.29
D	0.2 $CuCl_2$	0.2	0.05	-	0.25	0.88	1.20

Table 1. Initial salt concentration in precursor solution and metal ratios of annealed CZTSe absorber films.

Spray-deposited and Se-annealed CZTSe films showed characteristic reflections of the kesterite phase (PDF reference 01-070-8930) with a preferred orientation along the (112) direction as detected in the XRD pattern (Fig.2). Because ZnSe and Cu2SnSe3 exhibit very similar diffraction patterns, the presence of secondary phases cannot be excluded. In all sprayed and annealed CZTSe layers, we observed the formation of $MoSe_2$ caused by high selenium pressure during selenization.

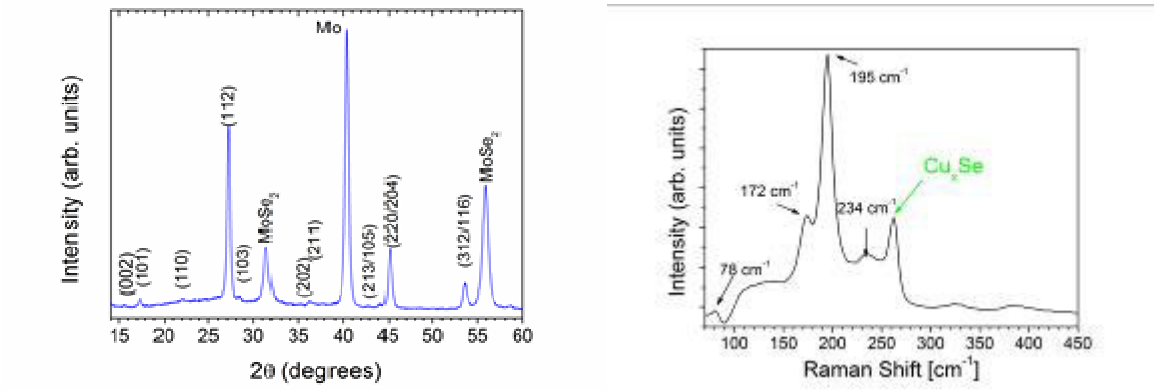

Fig.2. XRD pattern of sprayed CZTSe films (left). EDX gave a metal ratio Cu/(Zn+Sn)=0.88 and Zn/Sn=1.2. Raman (right) with HeNe laser, 633 nm, confirms kesterite phase and the presence of Cu_xSe phases.

Kesterite absorber by spin coating (Werner et al., 2015b) (Werner et al., 2015a)**:** EMPA has investigated the spin-coating approach of CZTSSe on Mo-coated soda lime glass. For the CZTSSe absorber film preparation, metal salts and 0.1 M NaCl were dissolved in DMSO not exceeding 3.5 M of total salt concentration, to target the metal ratios of Cu/(Sn+ Zn) =1.2 and Zn/Sn= 0.8. The precursor solution was spin-coated on Mo-coated soda lime glass substrate following a drying step at 320°C on a hot plate for one minute under atmospheric conditions. This step was repeated several times to build up the desired film thickness of the precursor. The precursor film was transferred to a rapid thermal process reactor. The annealing of the precursor took place in a closed graphite crucible with 0.7 g of Se pellets placed around the sample. All samples were selenised under a nitrogen base pressure of 850 mbar for 15 min at 500 ° C. The CZTSSe absorbers were KCN etched to remove possible binary phases.

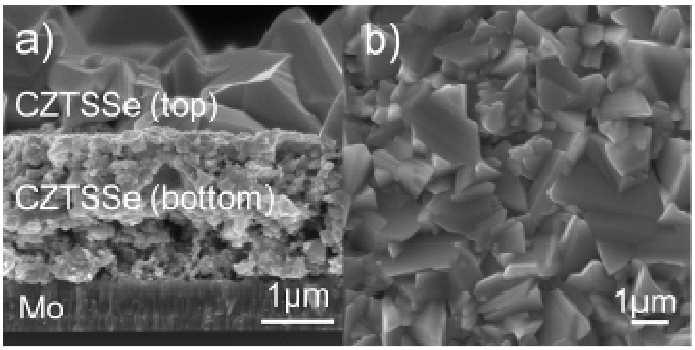

Fig.3. Typical SEM cross-section image (a) of a bi-layer CZTSSe absorber and (b) top view. The segregation of the large crystals of the top layer and the porous bottom layer are clearly visible.

The influence of NaCl in the precursor solution was investigated in detail. Annealing in an closed reactor results in a dense in the top crust and a bi-layer structure, with large grains at the top and a porous bottom layer. Figure 4 shows the SEM of a spin-coated and annealed in a graphite box CZTSSe absorber. The SEM cross- section does not reveal a visible change for the bottom layer upon additional NaCl. The FWHM is lower for samples with additional NaCl indicating an improved crystal quality in the presence of Na.

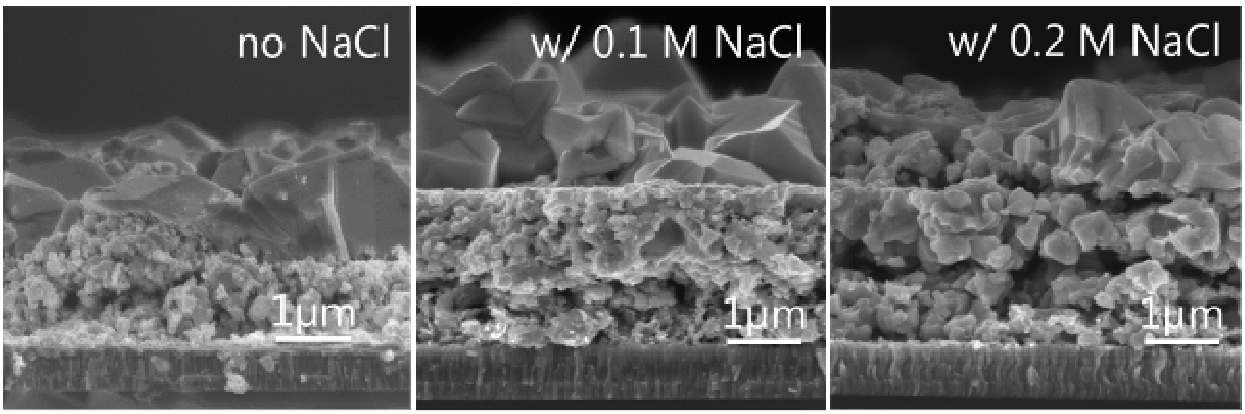

Fig.4. SEM cross-section image of Na (with different concentrations) treated CZTSSe absorber.

Different amounts of NaCl up to about 0.2 M were added to the solution and the precursors were thereupon annealed. The sodium concentration of 0.1 M NaCl is equivalent to ~ 90 nm thick top NaF layer. This concentration of 0.2 M could not be elevated further because it is limited by NaCl solubility in

DMSO. Lower concentration of 0.025 M and 0.05 M NaCl were also investigated but no significant difference in morphology or electronic properties as compared to sodium free precursor were observed.

The bi-layer structure continues to exist for absorber with 0.1 M NaCl additional in the precursor solution (Fig. 4) and a densification in the top crust was observed although the SEM cross- section does not reveal a visible change for the bottom layer. Upon an increase of NaCl concentration the absorber film changes to mono-layer with crystal of similar sizes.

Kesterite absorber by electrochemical deposition (ECD) (Wibowo et al., 2015)**:** This approach was pursued at AIT. Metal layers of Cu, Sn and Zn were deposited sequentially by galvanostatic electrodeposition on Mo-coated glass substrate with a platinized titanium mesh as counter electrode. The optimized, baseline solution compositions are reported in Table 2. The first layer on the Mo-coated glass was always Cu, while for certain samples the Zn and Sn sequence was interchanged. In galvanostatic deposition the current density is kept constant. This varied as a function of the deposited metal. The values that produced films with best properties were: 1.5 mA/cm^2 for Cu and Zn and 2 mA/cm^2 for Sn. The stoichiometry of the resulting multilayer stack was adjusted by the individual layer thickness, which was, in turn, controlled by the deposition time. The target was to achieve Cu-poor and Zn-rich compositions of: [Cu]/([Zn]+{Sn]) ~ 0.8 – 0.9 and [Zn]/[Sn] ~ 1.2 molar ratios.

Table 2. Detailed composition of used electrolytes

Electrolyte	Supporting electrolyte	Complex	Additive	pH
0.1 M $CuSO_4.5H_2O$	3 M NaOH	D-Sorbitol	-	14
0.08 M $SnCl_2.2H_2O$	0.12 M NaCl	0.65 M Na-citrate	1 mM PEG 200	5
0.1 M $ZnCl_2$	2.8 M KCl	0.32 M H_3BO_3	1 mM PEG 200	4

The first challenge was to obtain a Cu layer that adheres to the substrate and covers it homogeneously. This was achieved with an alkaline solution. Fig. 5(a) shows a SEM image from the surface of a 300 nm-thick Cu film. Small, homogeneous Cu grains, result in a highly reflective surface. The Sn and Zn layers were deposited on Cu resulting to the precursor multilayer. Fig. 5(b)-6(d) depict surface SEM images of Cu/Sn, Cu/Zn and Cu/Sn/Zn multilayers, respectively. Both Zn and Sn could be deposited on Cu with strong adhesion. The ECD of Zn on Cu results in a continuous film with homogeneous surface morphology (Fig. 5(c)). On the other hand, Sn on Cu forms large grains with island-like morphology with only partial coverage of the Cu surface (Fig. 5(b)). Fig. 5(e) presents a SEM image from the cleaved edge of the Cu/Sn/Zn sample.

X-ray fluorescence (XRF) was employed for analysis of the chemical composition of the precursors and chalcogenised films. XRF was previously calibrated with Inductively Coupled Plasma Optical Emission Spectrometer (ICP-OES). The films' structural properties were determined by XRD. The average, as-deposited precursor films' compositions, as extracted from ICP-OES measurements are summarized in Table 3. The films were prepared by varying Sn deposition time, while maintaining constant times for Cu and Zn depositions. The Sn deposition at 120 second finally provides the optimum metallic composition for kesterite.

All as-deposited precursors were polycrystalline and multiphase. The XRD patterns of Cu/Zn and Cu/Sn layers suggest formation of Cu_5Zn_8 / CuZn and Cu_6Sn_5 / $Cu_{41}Sn_{11}$ intermetallic compounds (IMC). Different behavior of Zn and Sn is obtained: in Cu/Zn films, Zn was entirely consumed by Cu to form Cu_5Zn_8 / CuZn, as denoted by the absence of any Zn reflections. On the contrary, although some part of Sn reacts to form Cu_6Sn_5, a substantial amount of Sn still remains unreacted in the Cu/Sn films.

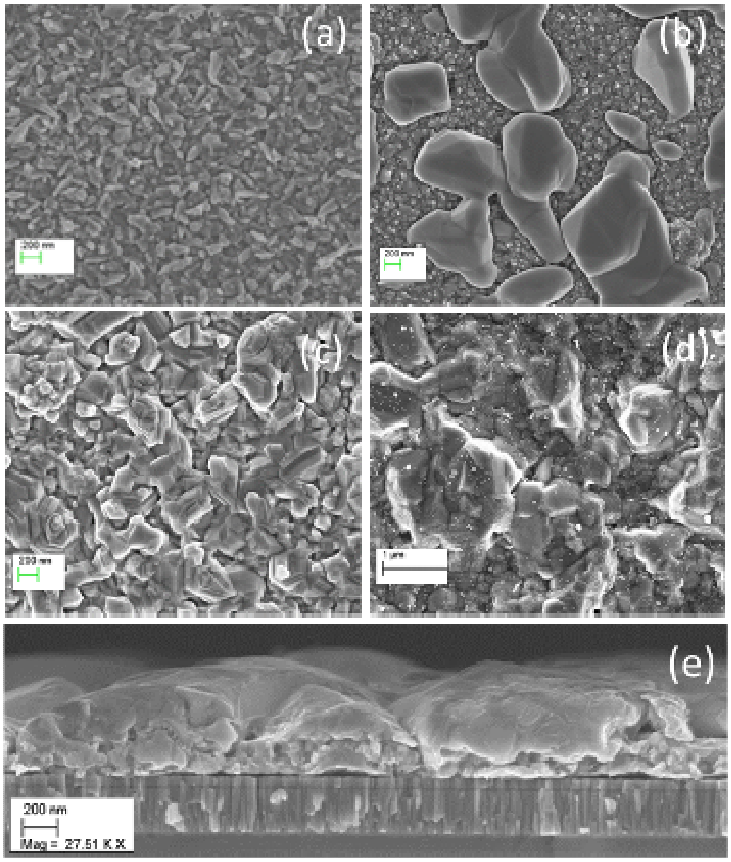

Figure 5: SEM images from the surface of: (a) Cu, (b) Cu/Sn, (c) Cu/Zn and (d) Cu/Sn/Zn. (e) Cleaved edge image from the Cu/Sn/Zn sample.

In the Cu/Sn/Zn precursor, where Cu and Sn are adjacent, the diffraction pattern reveals a dominant existence of brass, in the forms of CuZn and/or Cu_5Zn_8 phases with an elemental Sn phase. The Cu_5Zn_8 formation, which takes place during the deposition of Zn on the exposed Cu layer, is generally believed to be more dominant than that of Cu_6Sn_5 phase. The absence of an observable Cu_6Sn_5 principal reflection is an evidence of the preferential reaction between Cu and Zn instead of Cu and Sn.

Through chalcogenisation, the Cu/Sn/Zn precursors convert into $Cu_2ZnSn(S,Se)_4$. The investigation of the chalcogenised films showed that the metal relative compositions were significantly changed, particularly after the second stage of selenisation. The films suffered from Sn-loss, resulting in off-stoichiometric films, far below the targeted Cu/(Zn+Sn) = 0.8 and Zn/Sn = 1.2. The detailed composition of the chalcogenised films is summarized in Table 4. The loss of Sn may be attributed to the re-evaporation of volatile compound of Sn(S,Se) or $Sn(S,Se)_2$.

Table 3. Precursors composition as a function of Sn deposition time.

Sn deposition time (sec.)	Elemental composition (at. %)					
	[Cu]	[Sn]	[Zn]	[Cu]/([Zn]+[Sn])	Cu/[Zn]	[Zn]/[Sn]
80	48.8	18.8	32.4	0.95	1.50	1.72
100	47.3	22.1	30.5	0.89	1.55	1.38
120	46.6	23.9	29.5	0.87	1.58	1.23

Up to the sulfurisation stage, the metal precursors were converted into Cu_2ZnSnS_4 with excessive Zn and Sn (above 12.5 at.%) but very poor S (below 45 at. %). Selenisation stage produced films having very high chalcogens concentration and very low Cu and Sn concentrations. The cause for low Cu concentration in the chalcogenised films is not fully understood. But a $Cu_2(S,Se)$ detachment from the films can be a possible cause since this compound usually exists on the film surface. The compositions of as-chalcogenised films can be re-adjusted toward the ideal composition range by optimsing the chalcogenisation parameters.

Table 4. Chemical composition of as-chalcogenised films in at. %. The results from sulfurization stage are marked by the grey area.

Cu	Zn	Sn	S	Se	Cu/Zn	Cu/Sn	Zn/Sn	Cu/(Zn+Sn)	S/Metals	S/(S+Se)
27,06	14,25	16,64	0,02	42,02	1,90	1,63	0,88	0,86	0,00	1,00
18,73	18,29	19,37	0,03	43,58	1,02	0,97	0,50	0,94	0,00	1,00
27,12	19,43	19,01	0,02	34,42	1,40	1,43	0,71	1,02	0,00	1,00
12,74	11,95	8,86	52,62	13,83	1,07	1,44	0,61	1,35	1,57	0,21
14,43	9,49	9,22	56,71	10,16	1,52	1,57	0,77	1,03	1,71	0,15
12,68	12,11	8,88	52,46	13,86	1,05	1,43	0,60	1,36	1,56	0,21

The structural investigation by XRD of the as-chalcogenised films (Fig. 6) suggests that the films crystallised as kesterite-like structure (Fig. 7). Considering the results of the films' composition, it is believed that the films contain additional phases of ZnS, ZnSe or Zn(S,Se), which has identical diffraction pattern with kesterite and cannot be distinguished by XRD.

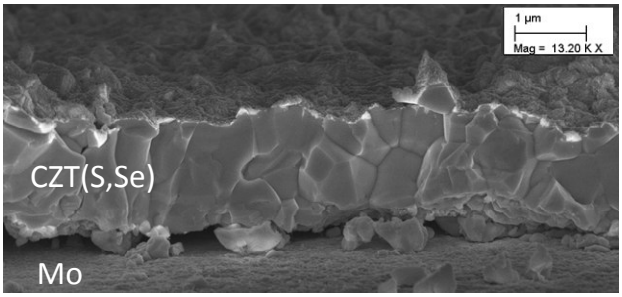

Fig. 6: Cross section SEM image of the as-chalcogenised CZT(S,Se) film.

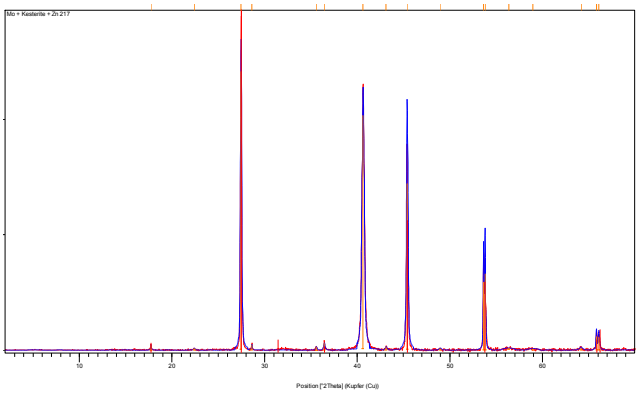

Fig. 7: X-Ray diffractogram of the CZT(S,Se) film.

In a next step, we have tried to control the CZTS film thickness through the adjustment of the metal precursor thickness. Thicker precursor films were prepared by increasing the Cu, Sn and Zn deposition times 30, 40, 50 and 60 % relative to the "baseline" process (described in Table 3). Unexpectedly, the first set of trials showed lower Cu content (< 41 at.%). Possibly this is due to the more pronounced Cu dissolution during the longer acidic Sn and Zn layer deposition. In order to compensate for the Cu dissolution, the targeted ratio of Cu/(Zn+Sn) in the precursor has been adjusted to 1, whereas the (Zn)/(Sn) ratio was kept at 1.2. The expected precursor thickness should increase proportionally with the deposition time. Due to the natural precursor surface roughness an accurate determination of the thickness was difficult. For this, the thickness and the composition of the precursor films were extracted from XRF measurements with an expected accuracy of 10%. The results are shown in Table 5.

Through the aforementioned adjustments, the as-deposited precursor composition is in the range of the desired Cu-poor and Zn-rich values of: Cu/(Zn+Sn) = 0.8 – 0.9 and (Zn)/(Sn) = 1.17 – 1.20. Neither film delamination nor presence of voids was observed. These results suggest three important technological aspects for the preparation of kesterite precursor films by electrochemical deposition: (i) the used electrolyte recipes lead to reproducible, high quality precursor films, (ii) the precursor composition can be tuned by controlling the deposition time and (iii) through the sequential deposition of Cu, Sn and Zn, precursor films with variable thickness can be achieved.

Table 5. Precursor thickness and chemical composition at various deposition times.

Increasing of total deposition time relative to baseline (%)	Thickness calculated from XRF (nm)	Elemental composition (at. %)					
		[Cu]	[Zn]	[Sn]	[Cu]/([Zn]+[Sn])	Cu/[Zn]	[Zn]/[Sn]
Baseline	562	50.64	29.11	20.25	1.03	1.74	1.44
30%	759	47.30	28.30	23.87	0.90	1.64	1.21
40%	726	47.55	28.88	23.57	0.91	1.64	1.23
50%	775	47.46	30.00	22.54	0.90	1.58	1.33
60%	850	46.03	29.03	24.90	0.85	1.58	1.17

Cu_2ZnSnS_4 (CZTS) films were prepared by annealing the precursor in an evacuated quartz tube under pure sulfur atmosphere. In this stage, optimization of kesterite film fabrication was performed by investigating the effect of annealing time and precursor thickness. An alumina crucible was employed as a sample holder where both Cu/Sn/Zn precursor and sulfur flake were placed into. Before annealing, the quartz tube was evacuated and purged with nitrogen. The crystallisation of Cu/Sn/Zn precursor to CZTS was optimised at heating rate of 10 °C/min and temperature of 560 °C for various annealing times. Annealing time was kept below 40 minutes due to the Sn-loss issue in the kesterite crystallisation. Moreover, the as-sulfurised film encounters severe delamination when annealed more than 40 minutes.

The films had a typical kesterite tetragonal phase as demonstrated by the X-ray diffractograms (Fig. 7). Increasing annealing time from 10 to 30 minutes enhanced crystallinity. Therefore, we conclude that the annealing time for crystallising metallic precursor into kesterite CZTS should not be too short in order to provide enough thermal energy for CZTS phase formation and not too long in order to prevent structural damage and/or re-evaporation of volatile elements or phases.

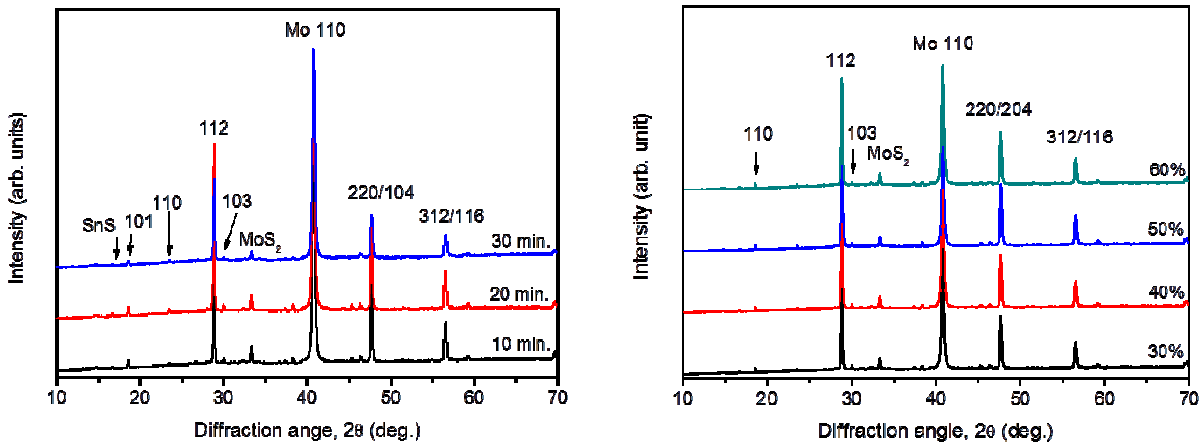

Fig. 7. (Left) X ray diffractogram of baseline CZTS films deposited at various annealing times. (Right) X-ray diffractogram of CZTS films annealed from various precursor film thickness.

The X-ray diffactrograms of as-sulfurised films suggest the presence of MoS_2 at the CZTS/Mo interface. In addition, SnS is also present, stemming from either incomplete sulfurisation of the precursor or from CZTS surface decomposition. Thicker precursors lead to higher degree of crystallinity, as can be seen from the relative intensity of the kesterite (1 1 2) reflection to the Mo (1 1 0) reflection. The

presence of ZnS phase cannot be excluded since the cubic zinc blende ZnS reflections overlap with the tetragonal kesterite CZTS reflections.

The thickness of the as-sulfurized films is larger than 1 µm, as shown by the SEM images in Fig. 8. Thicker CZTS films are obtained from thicker precursors. The CZTS films consist of relatively large grains (in the µm range) on the surface but exhibit smaller grains at the bottom, near the Mo/CZTS interface. This dual structure arises from the one-dimensional sulfurisation process which gradually starts from the precursor film's surface towards the bottom. As the film surface is exposed to longer sulfurisation time compared to the bulk and bottom, the surface experiences further recrystallization and grain growth, resulting to larger grains.

The CZTS films, however, still show voids in the interface between Mo and CZTS films. These voids can result in shunts in the complete solar cell. The thin layer of MoS_2 which is detected by XRD cannot clearly seen in SEM. From the microscopy studies using SEM, the presence of secondary phase of SnS is suggested from flake-like structures on the as-sulfurised surface.

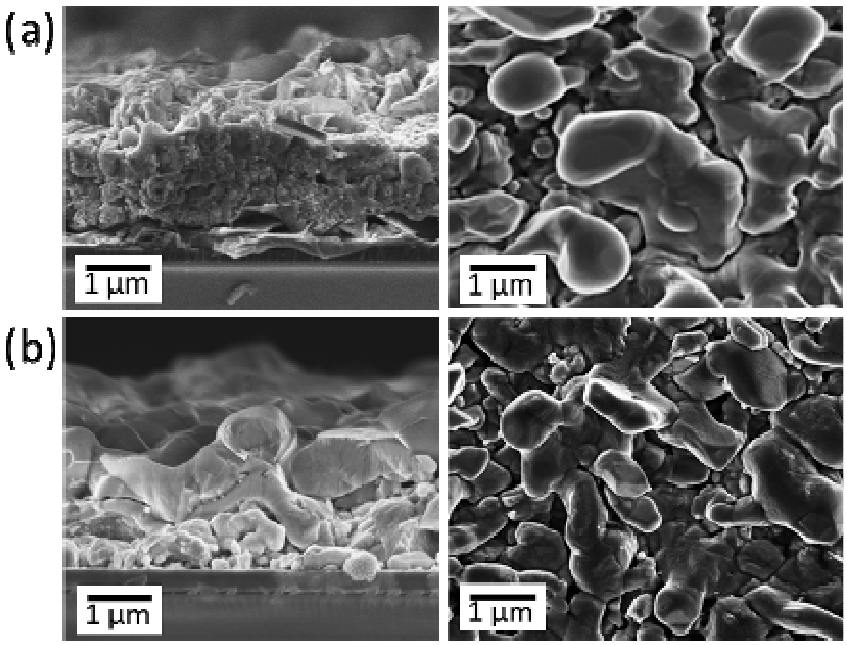

Fig. 8. CZTS absorber from increased precursor thickness relative to the "baseline": (a) 759 nm and (b) 726 nm.

ZnO and Al-doped ZnO (AZO) layer by chemical spray pyrolysis (CSP) (Edinger et al., 2015)**:** This approach was pursued in collaboration between AIT and EVG. ZnO and AZO layers were deposited by CSP on borosilicate glass, using exclusively aqueous solutions. The films were produced using an EVG®101 Advanced Resist Processing System with EVG's OmniSpray® coating technology. This setup was engineered and optimized for the specific deposition needs of the project. The solutions were atomized using an ultrasonic nozzle, which sprayed the droplet stream vertically onto the substrate. The depositions took place in ambient atmosphere in a clean room. In order to uniformly deposit the film on the whole substrate, the nozzle scanned over it along the x-axis and after each line-scan the hotplate moved in the y-axis. The film thickness was controlled by the number of the spraying cycles.

Before the deposition, the substrate was heated to the desired temperature, between 380 and 440 ^{o}C. The solutions contained zinc ions in 0.1 M concentration, provided either by solely ZnAc2 or a mixture of ZnAc2 and ZnCl2. The aluminum content was varied in the range between 0-3 mol% by adding $AlCl_3$ to the solutions. Acetic acid was also added in various concentrations between 0.1 and 10 vol%, in order to suppress zinc hydroxide precipitation in the solution. Predictions on the solution

stability were done using speciation diagrams. These suggested that for pH>6.5, zinc hydroxide precipitates, whereas for low pH values the concentration of zinc acetate declines.

In the first deposition series the pH value was adjusted at 4.3, different mixture ratios of ZnAc2/$ZnCl_2$ were used and dopant was introduced in certain cases in the form of $AlCl_3$. The deposited ZnO and AZO had many light-scattering defects. Their number was reduced with increasing the deposition temperature. Films deposited at lower temperatures had very pronounced porosity. On the contrary, the films deposited at 440 ^oC showed columnar ZnO growth. All films were highly resistive, with the lowest resistivity being 36 Ωcm for the film grown at 440 ^oC with 2% $AlCl_3$. From transmission measurements, we have extracted the direct bandgap of the ZnO and AZO layers between 3.27 eV and 3.34 eV. $ZnCl_2$ led to a drastic increase of structural artefacts, suggesting impingement of large droplets on the surface and growth of the film from the liquid phase. Therefore ZnCl2 was omitted from subsequent experiments and pure $ZnAc_2$ was employed as a source of Zn ions.

In the next deposition series the pH was reduced to 4 and a number of deposition parameters were put under test, such as the addition of dodecyltrimethylammonium chloride as surfactant to the solution, with the aim to decrease the droplet size distribution by lowering the surface tension. The surfactant should decompose upon arrival on the hot surface, as quarterny ammonium compounds generally are thermolabile. Additionally, the effect of ZnO pre-seeded substrates was investigated. Several improvements were also made in order to ensure growth quality and homogeneity over the substrate surface. These improvements included the introduction of short time intervals after each spraying cycle and the adjustment of the spray rate (varying from 5 to 50 μl/sec).

The decrease of solution pH reduced the films' defect density, resulting to high transparency and homogeneity throughout the surface of the glass slide. The films had the typical ZnO grain morphology in all cases. The X-Ray diffractograms of the layers showed peaks stemming from a plethora of crystal planes (100, 002, 101,…). The sheet resistance decreased significantly compared to the previous runs, which is consistent with the improved layer growth. For the sample containing 2% $AlCl_3$ a minimum resistivity of 3,3 Ωcm was attained. The use of surfactant led to the enlargement of the grain size but had a complex effect on the film resistivity, which depended on the presence of dopant in the solution. Because of this, the surfactant was omitted in further experiments. Instead, we employed other means to reduce the droplet size, as we will see below. Also, the presence of the ZnO seeding did not lead to significant growth effects, so following experiments were done on bare glass. On the other hand, a marked positive effect on the growth and electrical properties proved to have the introduction of the short time intervals between spraying cycles. Homogneous, columnar ZnO layers were obtained, with high transparency and low resistivity. The spray-rate mainly influenced the growth rate.

In the following experiments a time interval was introduced and the spraying rate was set at 10 μl/sec. Our investigation now concentrated on the effect of acetic acid concentration, which varied from 0.1 to 10 vol.%. One of the anticipated effects of increasing the HAc concentration in

water solutions is the decrease of the surface tension and the consequent reduction of the droplet size. An overview of solution compositions and of investigated samples is shown in Table 6. A first deposition series was conducted with 10 spraying cycles per solution (samples A-F). In a second deposition series, the number of spraying cycles was adjusted to obtain a film thickness of about 150 nm (samples A, G, H, I).

sample	HAc [vol%]	pH	*t* [nm]	RMS [nm]	*T* [%]	E_G [eV]	*ρ* [Ωcm]
A	0.1	5.51	140	7.9	83.7	3.28	1.19
B	2	4.12	110	5.1	83.7	3.30	0.22
C	4	3.82	100	4.7	82.2	3.30	1.50
D	6	3.65	83	4.9	82.2	3.30	2.97
E	8	3.50	87	5.9	82.5	3.30	4.59
F	10	3.36	85	6.1	83.2	3.28	9.07
G	2	4.12	160	9.1	80.5	3.29	0.36
H	4	3.82	150	10.4	83.3	3.29	2.15
I	6	3.65	145	8.7	83.4	3.29	2.33

Table. 6. Overview of samples, showing the acetic acid content in solution, the pH value of the solution, the sample thickness t, the RMS roughness value, the average direct transmittance T in the range of 400-1000 nm, the optical band gap EG and the thin films' resistivity values ρ .

In Fig. 9 we show typical SEM images from samples A, G, H and I. For low HAc concentration ZnO presents long, platelet-like grains, inducing pronounced roughness. With increasing HAc content, these elongated crystals become less distinct and yield to more regular, flat-top grains, with a denser morphology. Concomitant with this modification in the crystal morphology, a reduction of the thickness (*t*) was observed for acetic acid amounts of 0 to 6 vol% and constant spraying cycles, attaining a plateau for larger HAc content. This can be related to selective adsorption of HAc on specific surface facets. Indeed, carboxylic acids are known to adsorb onto 001-surfaces of ZnO. This can explain the initial decrease in growth rate with HAc concentration and the resulting higher vapor pressure of the acid at the substrate's proximity. Because of the latter, the adsorption probability of HAc rises and more sites are blocked on the growing film. However, once all relevant sites are blocked, the growth rate should stabilize, which was indeed observed in our experiments. As the growth at this surface is slowed down, this mechanism can also explain the observed change in grain morphology.

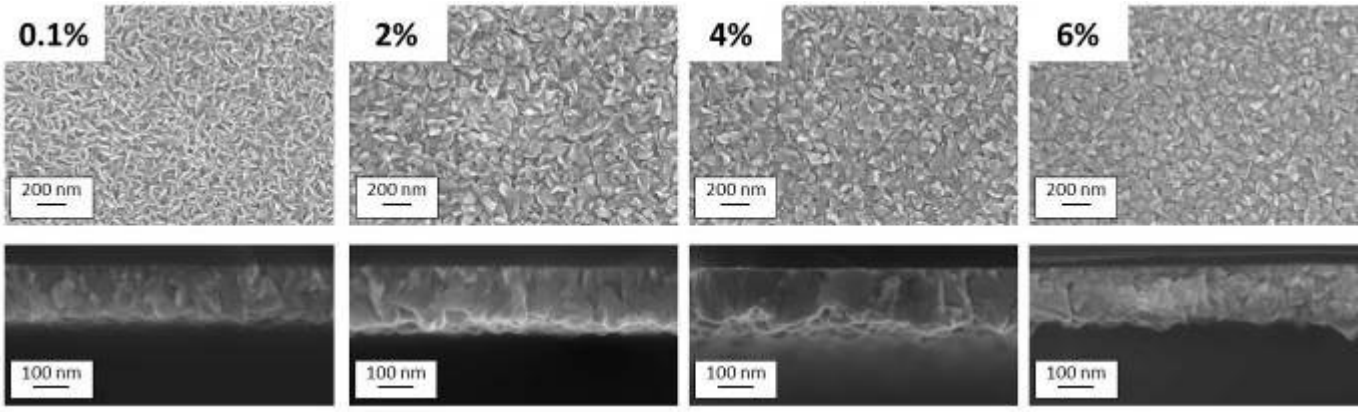

Fig. 9: SEM images for ZnO samples A, G, H and I.

The structural characterization (AFM and XRD) revealed that the grain size has a maximum for an HAc amount of 2 vol%, while the (001) texture of the ZnO films is enhanced with increasing amount of HAc. Despite these modifications in the films' texture, the optical properties are not significantly altered as seen in the UV-Vis spectra of Fig. 10. All films showed high transmittance of more than 80% in the range of 400 – 1000 nm. The optical band gap values, extracted from Tauc's plots, are in the range of 3.3 eV. This time, only a few, light-scattering artefacts can be observed.

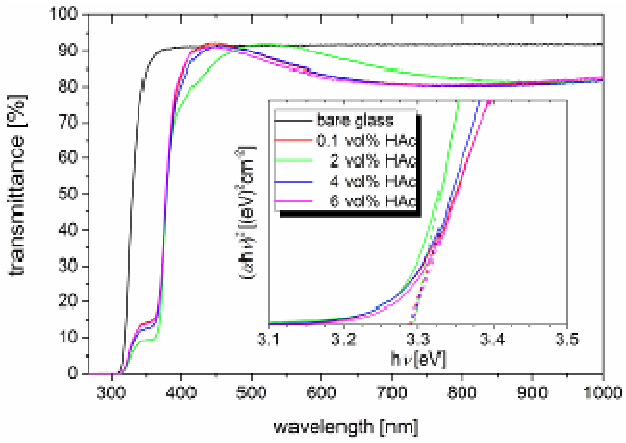

Fig. 10. UV-Vis spectra of A, G, H, I samples.

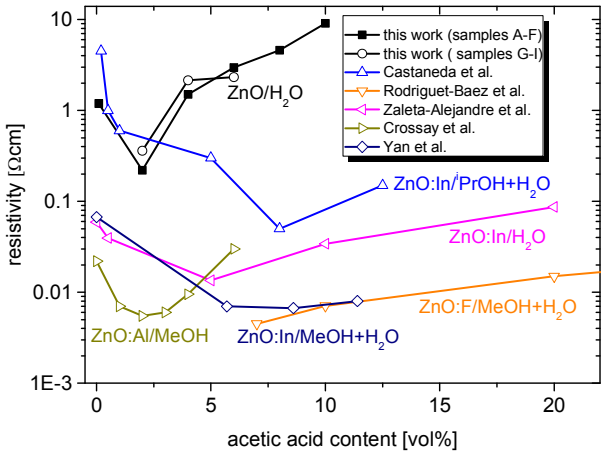

Fig. 11. Dependence of resistivity on HAc concentration.

The HAc concentration has a marked impact on the films' electrical properties. Due to the dependence of the resistivity values on the illumination, triggered by the UV-photodesorption of chemisorbed molecules in ZnO, we have decided to apply a pre-conditioning of the samples under controlled AM1.5G illumination conditions for 2 hours. This makes the comparison of resistivity values more consistent. During the illumination a continuous drop in resistivity was observed, which is attributed to the UV-part of the lamp spectrum. The dependence of the measured resistivity values (measured after illumination) on the amount of HAc is presented in Fig. 11. Our investigation shows consistently a minimum in resistivity for the 2 vol% films. A remarkable drop in the resistivity from ~1 Ωcm to ~0.2 Ωcm is obtained as HAc increases from 0.1 to 2 vol%. For larger

concentrations a continuous rise in the resistivity values is observed. This trend is in accordance with literature reports, which are also presented in Fig. 11 (Rodríguez-Báez et al., 2007), (Castañeda et al., 2006), (Yan et al., 2012), (Crossay et al., 2012), (Zaleta-Alejandre et al., 2012). They show that the electrical properties are strongly depending on the addition of HAc and most reports also point to a resistivity minimum between 2 and 8 vol%. The observed spreading in the position of the minimum is believed to arise from the different deposition conditions, especially concerning the growth temperature.

ZnO and Al-doped ZnO (AZO) layer by ECD: Parallel to the CSP technique, we have

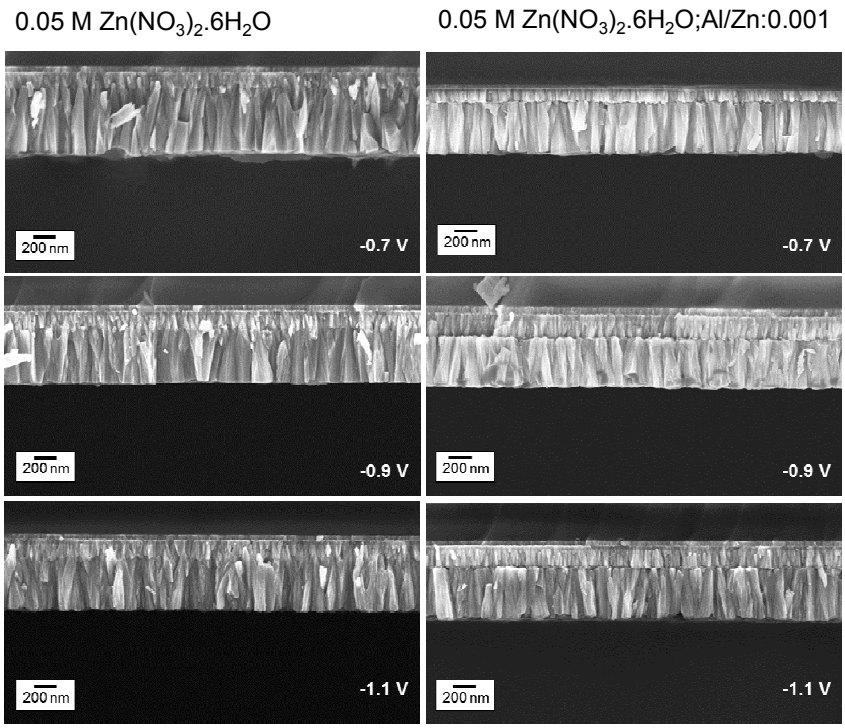

Fig. 12: SEM images from characteristic samples fabricated under different deposition potential.

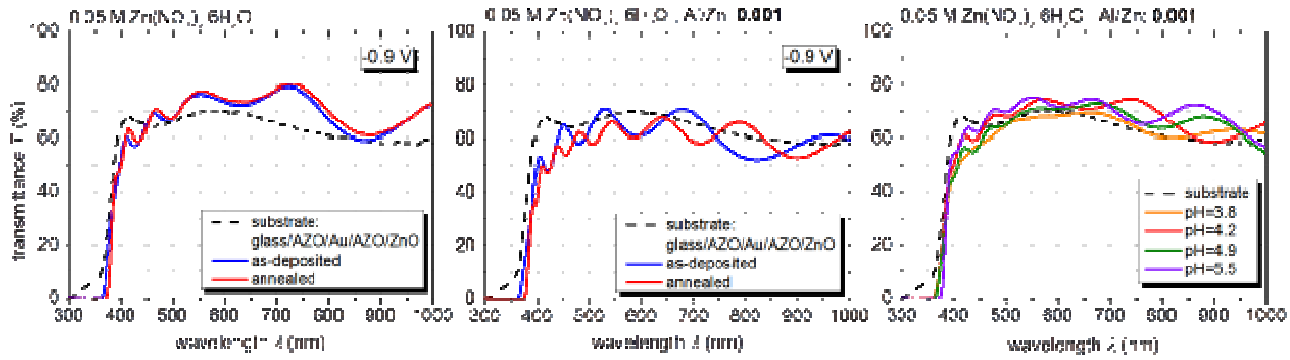

Fig. 13: UV-Vis transmission curves for selected ZnO and AZO films.

developed ECD for ZnO and AZO films. The deposition mode was potentiostatic, with conductive glass as working electrode, platinized titanium mesh as counter electrode and Ag/AgCl as reference electrode.

The main solution constituents were: de-ionized water, zinc nitrate ($Zn(NO_3)_2$) at molarities of 0.02-0.1 M and aluminum nitrate ($Al(NO_3)_3$) adjusted for ratios of Al3+/Zn2+= 0.001-0.01 in the solution. Due to the selective Al incorporation in the film, the Al concentration in the solution corresponds to a doping concentration of 1-10% in the film. The substrates were glass, covered with a sputtered, low resistive AZO-based electrode, which was covered with an intrinsic, highly resistive i-ZnO layer. The bath temperature was for most experiments 80 ^oC.

The range of potential values where ZnO deposition takes place was determined by cyclic voltammetry measurements. The samples were deposited at potentials between -0.6 and -1.1 V versus the Ag/AgCl electrode. Higher potential leads to denser nucleation sites on the substrate and, as a result, to more compact films. This is illustrated in Fig. 12 for ED-ZnO and AZO films at different deposition potentials. Intrinsic and low-doped layers are highly transparent, with a bandgap of 3.3-3.5 eV. For Al3+/Zn2+> 0.002, the obtained films have distorted growth and a milky appearance. The XRD characterization showed dominant (002) growth direction for all films. In further experiments, the effect of solution pH was investigated, in the region between 3.8 and 5.5 with the addition of HCl or NaOH, respectively (solution pH without any additive is 4.2). It was observed that films grown at higher pH were more compact, with more pronounced crystallinity.

In terms of conductivity of the ECD layers, it is very difficult to decouple it from the one of the conducting substrate. The sheet resistance of the whole multilayer varied between 79 and 19 Ω, with no clear tendency regarding the effect of the Al doping.

Buffer layers: Alernative buffer layers to CdS were also developed. Specifically ZnS by CSP and In2S3 by chemical bath deposition.

The goals for the ZnS CSP deposition were: (i) Find the best solvent for spraying ZnS buffer layer, (ii) find suitable mixture of precursors, (iii) check if additives are good for layer growth.

Experimental observations are as follows (EAM=Ethanolamine):

- Zn(OAc)2 (0.01M), TU (0.01M) in H2O + NaOH no precipitate was seen. (Zn2+ does not react with OH-)
- Zn(OAc)2 (0.01M), TU (0.01M), NH3 (0.5ml) in H2O cloudy solution, precipitate after 1h.
- Zn(OAc)2 (0.01M), TU (0.01M), EAM (0.1ml) in H2O forms immediately precipitates.
- Zn(OAc)2 (0.01M), TU (0.01M), EAM (0.1ml), NH3 (0.5ml) in H2O precipitates after spraying once.
- ZnCl2 (0.02M), TU (0.02M), EAM (0.2ml) in H2O precipitates.
- ZnCl2 (0.02M), TU (0.02M), NH3 (1ml), EAM (0.2ml) in H2O no precipitate
- ZnCl2 (0.02M), TU (0.02M), NH3 (1ml) in H2O no precipitate

Sample	Precursors	Solvent	Additives	Temperature [°C]	Spray time [min]	Layer thickness [nm]	Band gap
22.3	$ZnCl_2$ (0.02M); TAA (0.02M)	H_2O	-	350	40	20	3.771
22.4	$ZnCl_2$ (0.02M); TAA (0.02M)	H_2O	-	310	40	20	3.797

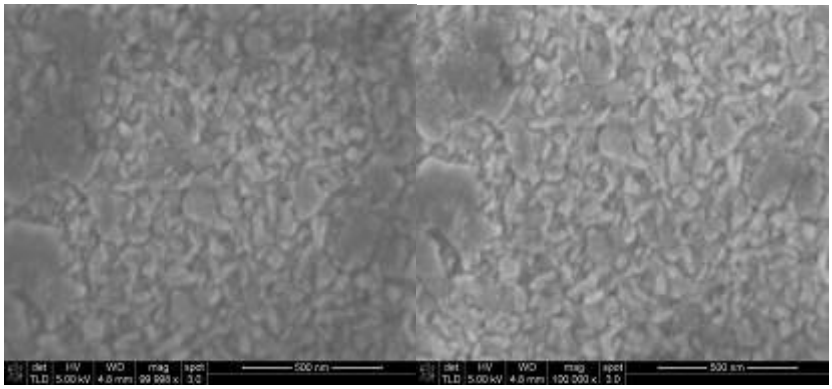

Fig. 14. Sample 22.3: Top views ZnS layer using $ZnCl_2$ and TAA shows dense, well crystalline layer, some cracks between grains sprayed at 310 °C.

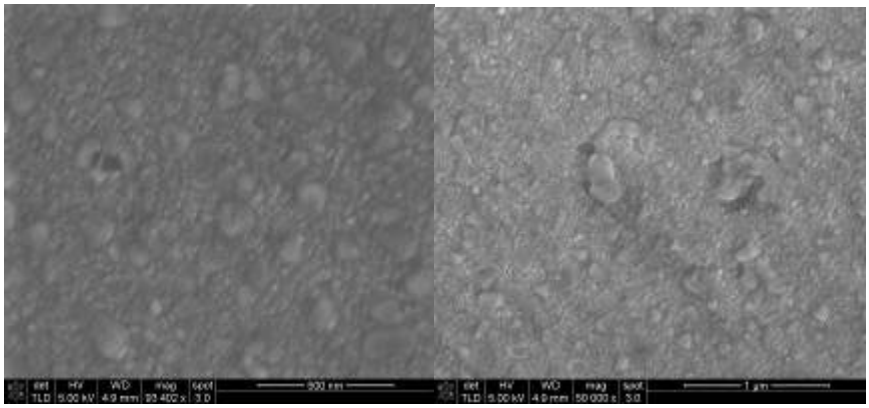

Fig. 15. Sample 22.4. Top views ZnS layer using $ZnCl_2$ and TAA shows denser layer than in 22.3, well sintered, no cracks between grains. Some larger grains are visible at 350 °C.

Conclusions:

- $ZnCl_2$ gives a layer at 300°C
- $Zn(OAc)_2$ gives a layer at 350°C
- $Zn(SO_4)$ does not give a layer at 350°C
- No growth could be observed if T was lowered by 50°C and acetone was used.
- Fast growth at 350°C (120nm after 40min)
- Higher T gives more crystalline (less amorphous) thin films. 350°C seems to be a good temperature to grow ZnS films: faster growth, more crystalline, not too high T.

We have also investigated an In_2S_3 buffer, grown by chemical bath deposition (CBD) on the CZTS absorber. The latter was produced by electrodeposition and subsequent chalcogenization. The In_2S_3 was selected as it provides a better energy band alignment with the CZTS as compared to ZnS. Before the buffer deposition the CZTS was etched in KCN solution to remove Cu_2S secondary phases from the surface. The bath for In_2S_3 deposition contained InCl3.4H2O, CH3COOH and thioacetamide, at a temperature of 70°C. The In_2S_3 film is of yellowish appearance, nanocrystalline character and homogeneous coverage. The optical characterization of the film showed an indirect bandgap of approx..

2 eV. SEM images from the surface of the glass/Mo/CZTS/ and glass/Mo/CZTS/In2S3 samples are shown in Figure 13(a) and 13(b) respectively.

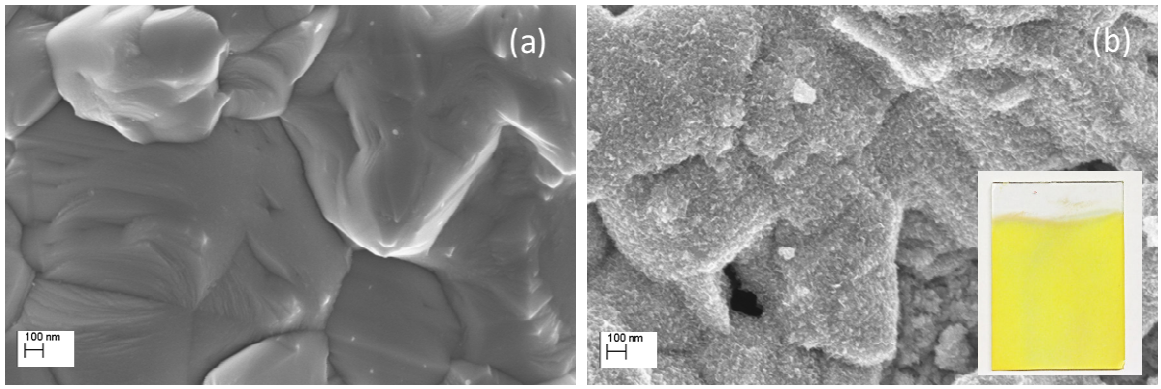

Fig. 13. (a) Surface of the CZTS absorber. (b) Surface of the CBD-grown In_2S_3 on top of CZTS and a photo of the In2S3 layer on glass (inset).

Integration of materials into solar cells: Solar cells were fabricated by chemical spray pyrolysis and their performance was compared to reference cells with spin-coated absorber. KCN etching was performed to remove possible binary Cu_xSe phases. CdS buffer was then deposited by chemical bath deposition on top of the CZTSe layer. Subsequently, an i-ZnO/ZnO:Al window bi-layer was RF magnetron sputtered, followed by mechanical scribing of individual cells of 0.09 cm2. Current–voltage (I–V) measurements were performed under standard test conditions (AM 1.5G spectrum, 25 °C). Solar cells were processed from annealed CZTSe absorber layers with a total metal ratio of Cu/(Zn+Sn)=0.88 and Zn/Sn=1.2 (EDX).

Solar cells were also fabricated by ECD CZTS(Se), with or without In2S3 buffer and sputtered ZnO/AZO window/TCO combination. A SEM image from such a cell is presented in Fig. 14.Unfortunately , ECD cells suffered from shunts, preventing PV performance measurements.

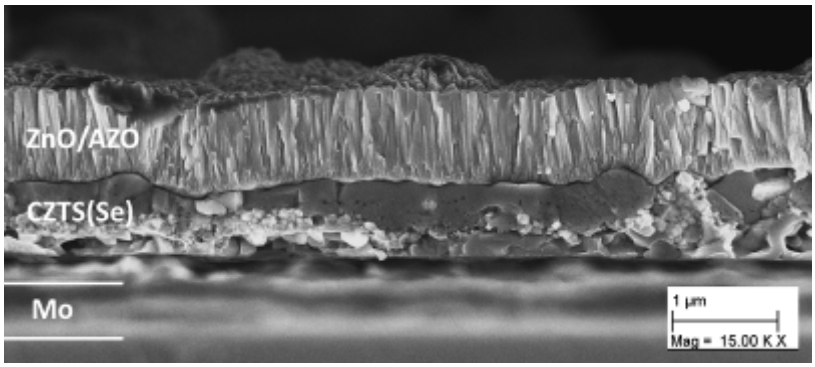

Fig. 14: A complete solar cell of glass/Mo/ECD-CZTS(Se)/ZnO/AZO.

Fig. 15 shows the J-V curve of sample D of Table 1, the film with the highest obtained conversion efficiency for sprayed kesterite absorbers of 0.7% on a 0.09 cm2 area.

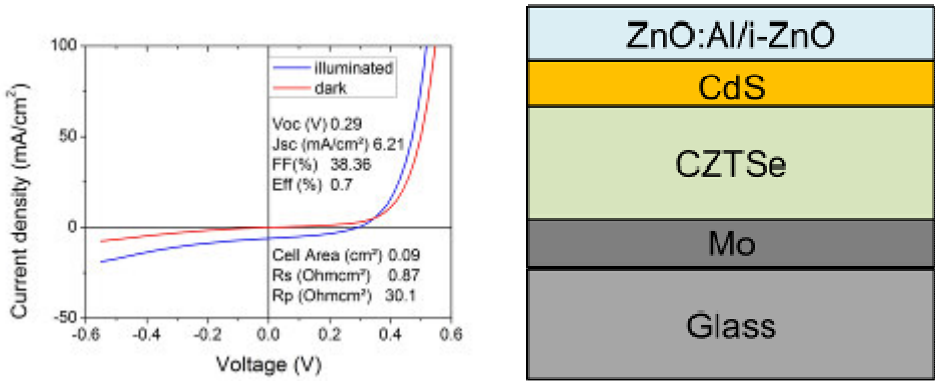

Fig.15. J-V curves of CZTSe absorber solar cell under illumination and dark conditions and typical schematic view.

The J-V characteristics and the external quantum efficiency of the reference, spin-coated cell are shown in Fig. 16.

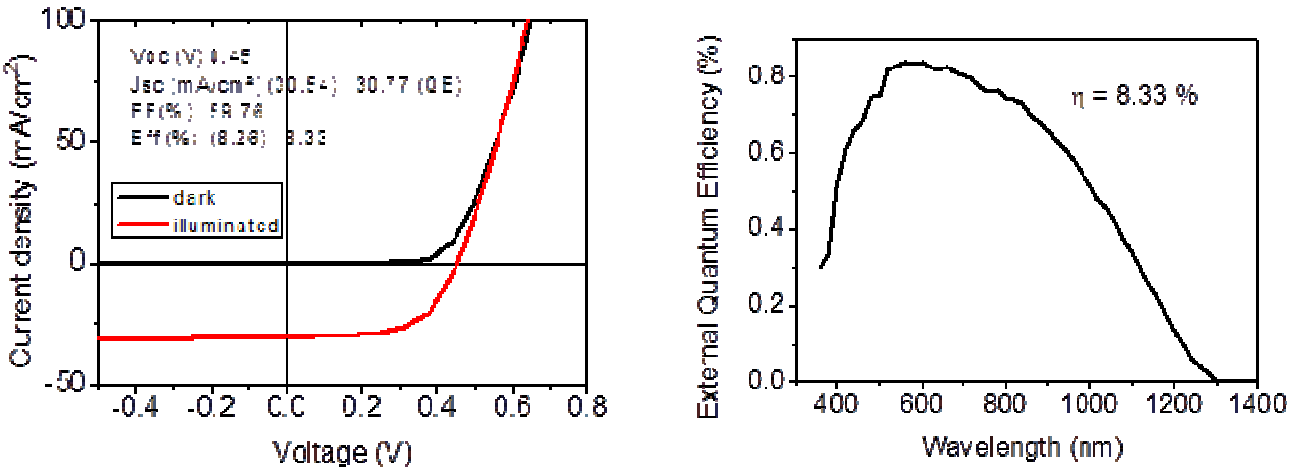

Fig.16. J-V characteristic of best performing solar cell (spin coating) from with a total area of 0.09 cm^2 under dark and illuminated conditions and EQE of the same cell.

It was possible to improve the efficiency to 8.3 % (cell area 0.09 cm^2, no antireflection coating) by adding NaCl to the solution. Dark and illuminated I-V curves of the best cell are presented in Fig. 16. The EQE measurements in Fig. 16 yield the highest current Jsc = 30.77 mA/cm^2, which is in a good agreement with results from I-V measurements. We assume that sodium located primarily at the grain boundaries can passivate donors and deep defects resulting in reduced recombination which would manifest itself in an increased Voc and FF (Kronik et al., 1998).

4 Ergebnisse und Schlussfolgerungen

The main results of the project are:

- We demonstrated CZTS(Se) absorber layer sprayed in a sequence of Cu-, followed by Zn-, Sn- and sulfur-containing alcoholic solutions. Sequential spraying provides a greater flexibility in terms of molarity and reduces the possibility of instable solutions. The effect of different sulfur source on the Zn/Sn metal ratio was investigated and a reduction of Zn loss was found when using thioacetamide. Reducing the Sn concentration led to the desired Zn-rich film formation.
- CZTSe absorber with state-of-the-art properties was developed by spin-coating metal salts dissolved in DMSO solution and subsequent selenization. The effect of sodium content in improving the CZTSe properties was demonstrated.
- We demonstrated that high quality metallic precursor layers for CZTS(Se) can be deposited electrochemically, using mild aqueous solutions and low temperatures. The stoichiometry of the metals in the final kesterite absorber can be tuned by adjusting their respective layer thickness. Kesterite films could be obtained after the chalcogenization process.
- Buffer layers of ZnS and In_2S_3 with appropriate properties were developed by chemical spray pyrolysis and chemical bath deposition, respectively, as alternatives to the standard CdS buffer.
- Transparent and conductive ZnO and aluminum-doped ZnO (AZO) layers were developed using electrochemical deposition, from aqueous solutions and temperatures below 90^{o}C.
- ZnO, and aluminum-doped ZnO layers were developed by the spray pyrolysis technique from exclusively water-based solutions, at temperatures below 400 ^{o}C and with high quality structural, optical and electrical properties.
- CZTSe solar cells formed by spray pyrolysis showed an energy conversion efficiency of 0.7%. CZTSe cells formed by spin coating showed efficiency larger than 8%. ECD-grown kesterite cells suffered from shunts. The work for addressing the shunt issue is currently on-going.

The main conclusions of the project are as follows:

- The chemical spray pyrolysis method for CZTS(Se) is feasible but not suitable for producing efficient absorber films. On the contrary, the spin-coating technique is the solution process of choice for efficient CZTS(Se) solar cells.
- The sequential potentiostatic electrodeposition of metallic thin film precursors is a very promising technique for kesterite CZTS(Se) absorber, since it is upscalable, uncomplicated in terms of solution preparation, we can easily adjust the composition through the thickness of the metallic constituents and the deposition takes place close to room temperature.
- Alternative buffer layer, such as ZnS, is not yet capable to replace CdS in producing efficient CZTS(Se) cells.
- It is possible to produce intrinsic and doped-ZnO layers using exclusively water-based solutions, with layer properties similar to solutions with alcohol-content. Water-based solutions greatly facilitate the processing, as the high temperatures used for spray pyrolysis demand strict safety measures when an alcohol-containing solvent is employed.
- Compact and highly transparent ZnO and doped-ZnO layers can be fabricated by ECD.
- It is possible to prepare a complete solar cell using exclusively low-cost, solution-based processing for all components, i.e. transparent contact, absorber, buffer.

5 Ausblick und Empfehlungen

Based on the presented results, it is demonstrated that CZTSSe, buffer layers and transparent conducting oxide films can be fabricated using the aforementioned proposed solution-based processes. For what concerns the ECD kesterite fabrication approach, the critical step for the film fabrication was the adjustment of the electrolyte composition to prepare the metallic Cu/Sn/Zn precursor at the correct Cu-poor and Zn-rich composition. Nevertheless, the achieved results presented in this report also dictate several important tasks that should be addressed in future works towards the goal of achieving efficient kesterite solar cells.

(a) The fabrication of CZTSSe films obviously depends on the chalcogenisation process as the most critical process where crystallization of the metallic precursors takes place into a single phase with the desired chemical composition. The present approach of chalcogenisation employing a closed container with a chalcogen source (powder or flakes) is not necessarily suitable for large scale fabrication in a continuous process. Thus, a systematic investigation to adapt the present chalcogenisation approach into a more practical and high-throughput-compatible approach is definitely required. In addition, a chalcogenisation approach using rapid thermal processing can also be proposed in order to eliminate the presence of secondary phases at the end stage of chalcogenisation, as well as to reduce the necessary time for the chalcogenisation process.

(b) It has been observed that during the chalcogenization process selective loss of materials takes place, which eventually needs to be compensated to achieve the proper kesterite phase. How to compensate for such loss most efficiently (e.g. by the targeted addition of metal sulfides during the crystallization process) is an open research question, which can be the subject of further studies.

(c) The choice of buffer layer material is very decisive and cannot be limited to the ZnS and In2S3 options to replace the standard CdS (containing toxic Cd). As non-heavy metal-containing buffer layers have been envisioned to be applied in the CZTSSe thin film photovoltaics, a dedicated study on the fundamental aspects of interface band alignment between kesterite and various candidate materials needs to be taken into consideration, supported by both simulation and experimental work. Indeed the ZnS suffers from poor conduction band alignment with the kesterite and In2S3 contains the rare element indium. So, if large scale implementation is considered In2S3 has also to be replaced by another abundant material.

(d) Solution-based TCO fabrication remains an extremely important topic and relevant to any thin film photovoltaic technology. Although significant progress has been marked lately in this field, there still remain great challenges regarding the stability of the solution-based TCOs and the role of the dopant on the structural, electrical and optical properties. To this end, vacuum-processed TCOs still remain today state-of-the-art. In SOLO-PV we have shown that CSP and ECD are suitable processes for producing ZnO-based TCOs. Nevertheless, the dopant incorporation and the stability of the resistance still remain issues that must be further investigated in future collaborative projects. Apart for the Al dopant, other donor elements have to be explored in relation to the aforementioned process.

6 Literaturverzeichnis

Castañeda, L., García-Valenzuela, A., Zironi, E.P., Cañetas-Ortega, J., Terrones, M., Maldonado, A., 2006. Formation of indium-doped zinc oxide thin films using chemical spray techniques: The importance of acetic acid content in the aerosol solution and the substrate temperature for enhancing electrical transport. Thin Solid Films 503, 212–218. doi:10.1016/j.tsf.2005.12.263

Crossay, A., Buecheler, S., Kranz, L., Perrenoud, J., Fella, C.M., Romanyuk, Y.E., Tiwari, A.N., 2012. Spray-deposited Al-doped ZnO transparent contacts for CdTe solar cells. Sol. Energy Mater. Sol. Cells 101, 283–288. doi:10.1016/j.solmat.2012.02.008

Edinger, S., Bekacz, J., Richter, M., Hamid, R., Wibowo, R.A., Peić, A., Dimopoulos, T., 2015. Influence of the acetic acid concentration on the growth of zinc oxide thin films prepared by spray pyrolysis of aqueous solutions. Thin Solid Films. doi:10.1016/j.tsf.2015.04.027

Kronik, L., Cahen, D., Schock, H.W., 1998. Effects of Sodium on Polycrystalline Cu(In,Ga)Se2 and Its Solar Cell Performance. Adv. Mater. 10, 31–36. doi:10.1002/(SICI)1521-4095(199801)10:1<31::AID-ADMA31>3.0.CO;2-3

Rodríguez-Báez, J., Maldonado, A., Castañeda, L., Delgado, G.T., Castanedo-Pérez, R., de la L. Olvera, M., 2007. On the effect of acetic acid on physical properties of chemically sprayed fluorine-doped ZnO thin films. Thin Solid Films 515, 8689–8694. doi:10.1016/j.tsf.2007.03.132

Werner, M., Sutter-Fella, C.M., Hagendorfer, H., Romanyuk, Y.E., Tiwari, A.N., 2015a. Cu $_2$ ZnSn(S,Se) $_4$ solar cell absorbers processed from Na-containing solutions in DMSO: Cu $_2$ ZnSn(S,Se) $_4$ solar cell absorbers. Phys. Status Solidi A 212, 116–120. doi:10.1002/pssa.201431146

Werner, M., Sutter-Fella, C.M., Romanyuk, Y.E., Tiwari, A.N., 2015b. 8.3% efficient Cu2ZnSn(S,Se)4 solar cells processed from sodium-containing solution precursors in a closed reactor. Thin Solid Films 582, 308–312. doi:10.1016/j.tsf.2014.10.043

Wibowo, R.A., Hamid, R., Maier, T., Dimopoulos, T., 2015. Galvanostatically-electrodeposited Cu–Zn–Sn multilayers as precursors for crystallising kesterite Cu2ZnSnS4 thin films. Thin Solid Films 582, 239–244. doi:10.1016/j.tsf.2014.10.060

Yan, W., Tan, J., Zhang, W., Meng, X., Lei, T., Li, C., Sun, X., 2012. Tailoring the structure and properties of ZnO:In films by different kinds of acids. Mater. Lett. 87, 28–30. doi:10.1016/j.matlet.2012.07.061

Zaleta-Alejandre, E., Camargo-Martinez, J., Ramirez-Garibo, A., Pérez-Arrieta, M.L., Balderas-Xicohténcatl, R., Rivera-Alvarez, Z., Aguilar-Frutis, M., Falcony, C., 2012. Structural, electrical and optical properties of indium chloride doped ZnO films synthesized by Ultrasonic Spray Pyrolysis technique. Thin Solid Films 524, 44–49. doi:10.1016/j.tsf.2012.09.050

7 Kontaktdaten

Theodoros Dimopoulos

AIT-Austrian Institute of Technology, Energy Department, Photovoltaic Systems

Giefinggasse 2, 1210 Vienna; Tel: +43 664 825 1317 ; F +43 50550-6390 ;

e-mail:theodoros.dimopoulos@ait.ac.at ; www.ait.ac.at.

Yaroslav Romanyuk

EMPA, Laboratory fort hin Films and Photovoltaics, Dübendorf, Switzerland

Anneliese Pönninger

EV Group (EVG), St. Florian am Inn, Austria

IMPRESSUM

Verfasser
AIT-Austrian Institute of Technology, Energy Department, Photovoltaic Systems
Giefinggasse 2, 1210 Vienna
Tel: +43 664 825 1317
Fax: +43 50550-6390
E-Mail:theodoros.dimopoulos@ait.ac.at
Web: www.ait.ac.at.

Eigentümer, Herausgeber und Medieninhaber
Klima- und Energiefonds
Gumpendorfer Straße 5/22
1060 Wien
E-Mail: office@klimafonds.gv.at
Web: www.klimafonds.gv.at

Projektpartner und AutorInnen
Austrian Institute of Technology
- Theodoros Dimopoulos
- Stephan Abermann
- Rachmat Adhi Wibowo

Empa, Materials Science and Technology
- Yaroslav Romanyuk
- Melanie Werner

EV Group
- Anneliese Pönninger

Gestaltung des Deckblattes
ZS communication + art GmbH